Thermal conductivity of amorphous solids above the plateau: Molecular-dynamics study

J. Michalski*
Institute of Theoretical Physics, University of Lausanne, CH-1015 Lausanne, Switzerland
(Received 23 August 1991; revised manuscript received 18 November 1991)

The thermal conductivities of two-dimensional crystalline, amorphous, and quasicrystalline classical models are studied via the nonequilibrium molecular-dynamics method. The behavior of the high-temperature thermal conductivities of crystal and glasses are reproduced. The difference between the thermal conductivities of the crystalline and amorphous models is explained by the presence of localized vibrational modes found in the latter. The results support the model of anharmonicity-induced hopping heat transfer in glasses. The thermal conductivity of the quasicrystalline model does not differ from that of the amorphous model, suggesting that the effect of quasiperiodicity on the thermal conductivity is the same as that of a simple aperiodicity. It is shown that localized modes are at the origin of strong anharmonicity of amorphous solids. This anharmonicity, together with the localization, influences the spectral intensities, which have several peaks instead of one.

I. INTRODUCTION

The thermal conductivity of amorphous solids is not well understood in any temperature range. It differs very much from that of crystals. One can distinguish three characteristic temperature intervals: (a) low T ($T \lesssim 1$ K), where $\kappa(T) \sim T^{1.8-2.0}$; (b) medium T ($T \approx 10$ K), where the thermal conductivity is constant (plateau); and (c) high T ($T > 10$ K), where κ rises smoothly to a limiting value $\kappa(\infty)$ given by the kinetic formula

$$\kappa = \tfrac{1}{3} C v l \ , \tag{1}$$

where l is the mean free path, of the order of interatomic distance, v the velocity of sound, and C the classical specific heat (see Fig. 1).

It is surprising that the thermal conductivity of amorphous solids depends very weakly on the structure and chemical composition.[2] Amorphous materials as different as, for example, SiO_2, Se, disordered crystals, and polymers have very similar thermal conductivities. This fact suggests that the explanation of the thermal conductivity of amorphous solids must be independent of structural details or the vibrational spectrum. The only common feature of all amorphous solids is their aperiodicity. In this paper we demonstrate that aperiodicity alone is enough to explain qualitatively the thermal conductivity of glasses at high temperatures ($T > 10$ K). We also show that the vibrational localization, which arises from the aperiodicity, is at the origin of the strong anharmonicity of amorphous solids.

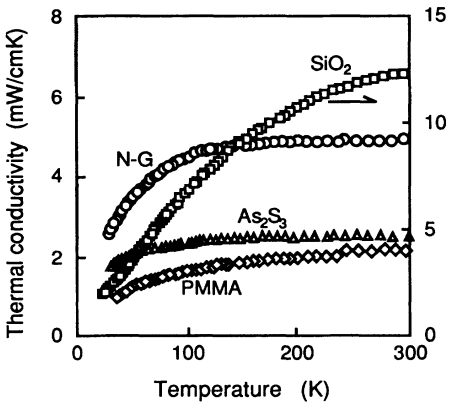

FIG. 1. Thermal conductivity for temperatures above the plateau temperature for four amorphous solids (from Ref. 1). The data for vitreous silica are plotted according to the scale on the right.

This paper is organized as follows. In Sec. II we review different theoretical models intended to explain thermal conductivity above the plateau. In Secs. III–VI, we present our molecular-dynamics simulation of the thermal conductivity of classical periodic and aperiodic models. In Sec. VII we study vibrational properties of our models and explain our results for the thermal conductivity by the localization and anharmonic interaction of vibrational modes (part of the contents of Secs. III–VII has already been communicated.[3] In Sec. VIII we present our simulation of the thermal conductivity of a model, quasiperiodic in one direction, in order to answer the question of whether or not the influence of quasiperiodicty on the thermal conductivity is different from that of a simple aperiodicity. In Sec. IX we show how a strong anharmonicity results from the vibrational localization and what influence both of these have on the spectral intensities of the normal modes. In Sec. X we discuss the theoretical models presented in Sec. II in the light of our results.

II. REVIEW OF THE THEORETICAL MODELS

A mechanism by which the thermal conductivity of amorphous solids increases with temperature above 10 K has been proposed by Alexander, Entin-Wohlman, and Orbach.[4] According to their proposal, the connectivities

of the bonds in amorphous solids have fractal geometry at short length scale (i.e., at distances shorter than a critical length l_{cr}). At long length scale, the structure is Euclidean. Low-frequency phonons whose wavelengths are longer than the critical length are not affected by the fractal structure and can be well described by the Debye model. High-frequency vibrations are "fractons"—vibrations of fractals.[5] Fractons are localized and cannot participate directly in the transport of energy at low temperatures. At higher temperatures ($T \gtrsim 10$ K), the fractons can contribute indirectly to heat transport by exchanging energy by means of anharmonic interactions (hopping conductivity). This mechanism gives the thermal conductivity, which first increases linearly with temperature and then saturates at a constant value when the lifetime of fractons becomes comparable with the period of their vibrations.[6] Even if the fracton wave function alone has been used to represent the localized vibrations in the calculation of the thermal conductivity, one would expect the same results to hold for more conventional vibrations localized above some critical frequency ω_c.[6]

A quite different mechanism has been proposed by Karpov and Parshin.[7] According to these authors, at temperatures above the plateau temperature, the heat is transported by phonons of frequencies $\omega \ll k_B T/\hbar$. These phonons are scattered resonantly by two-level systems, with the population of level differences proportional to $1/T$. The phonon mean free path then grows linearly with increasing T. As a result, the thermal conductivity increases linearly with temperature, as in the fracton model. Both models give the same qualitative results, but they are based on completely different mechanisms: In the fracton model, the augmentation of the thermal conductivity is due to an *additional heat transport* introduced by the anharmonic interactions, whereas in the other model, this augmentation is explained by a *diminution of the phonon scattering.*

A very simple qualitative explanation of the thermal conductivity of amorphous solids above the plateau was proposed by Kittel.[8] According to this, the phonons are scattered so strongly by the structural disorder that their mean free path is the shortest possible and is equal to the interatomic distance a. If one uses the kinetic formula [cf. (1)] $\kappa = \frac{1}{3} Cva$, one sees that the thermal conductivity increases with the specific heat C. This qualitative explanation is not satisfactory because the kinetic formula is applicable only where one can assign a velocity v to phonons. This is not possible if the mean free path is shorter than the wavelength. Moreover, in amorphous solids, the high-frequency vibrations are localized and cannot propagate. Nevertheless, Allen and Feldman,[9] who used the Kubo formula to calculate the thermal conductivity of the Wooten-Winer-Weaire model of amorphous silicon,[10] found a thermal conductivity that agreed well with the Kittel model. Unfortunately, their results were not in quantitative agreement with experiment[1,11] (they were too small), but Allen and Feldman attributed this to the fact that low-frequency modes were absent from their calculations because of the small size of the system studied (216 atoms in a cubic box).

III. DESCRIPTION OF THE PERIODIC AND APERIODIC MODELS

In order to be able to decide which properties of amorphous solids are responsible for their thermal conductivity above the plateau and to verify the models described in the previous section, we undertook a molecular-dynamics simulation of thermal flux through two two-dimensional classical (i.e., not quantum mechanical) models of a periodic (crystalline) and an aperiodic (amorphous) solid, respectively. The two models are very similar—they are both modifications of the Penrose tiling.[12,13] The choice of the Penrose tiling as the basis of our models was prescribed by the facility it affords to construct the aperiodic model from the periodic in such a way that the topology and orientational order of the bonds are the same for both models. Therefore the possibility of details of local structure being responsible for the difference in thermal conductivity of the models (see Sec. V, in particular Fig. 5) may be excluded. Similarly, our choice made it possible to compare the thermal conductivity of the quasiperiodic model (Sec. VIII) with those of the periodic and aperiodic ones. First, we will describe the periodic model in detail, and then we will define the amorphous model in relation to the periodic one.

The periodic model (PM) consists of 8 unit cells of 50 atoms each, which form a strip (see Fig. 2). Each unit cell is a so-called $\tau=2$ periodic approximant of the Penrose tiling with $F_x = F_y = 2$ and the grid parameters $\gamma_i = 0.5$, $i = 1, \ldots, 5$ (see Appendix A). Atoms are placed at the vertices of the tiling and are coupled to each other by springs along the sides and also along the short diagonals of the rhombi. We added these short diagonals to make the system more rigid and avoid large stringlike vibrations of the strip. In this way one obtains bonds of three different lengths r_i ($i = 1,2,3$), numbered in the order of increasing length. r_2 is the length of the rhombus side, $r_1 = (\tau - 1) r_2$, $r_3 = 2(1 - \tau^2/4)^{1/2} r_2$, $\tau = \frac{1}{2}(1 + \sqrt{5})$ being the golden number. All bonds are oriented along one of the side directions of a single regular pentagon or along lines pointing to the vertices of the same pentagon. Even if the orientational order of the bonds is not "crys-

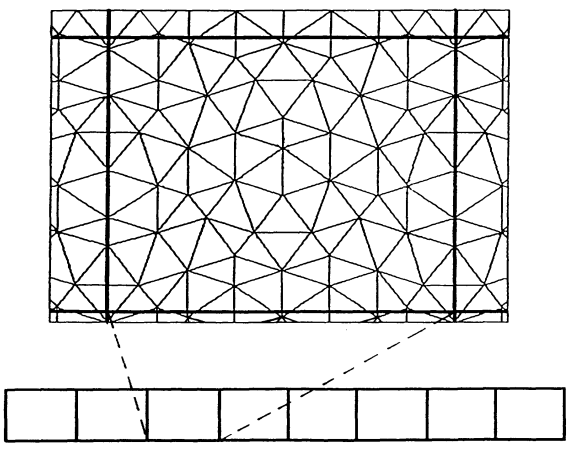

FIG. 2. Unit cell of the periodic model.

tallographic," the unit cell is rectangular and the system composed of such unit cells is crystalline (periodic).

The dimensions of the unit cell are $L_x \times L_y$, with

$$L_x=[3(1+\tau^2)^{1/2}+2(1-\tau^2/4)^{1/2}]r_2=6.881\,91r_2$$

and $L_y=(3\tau+1)r_2=5.8541r_2$. The "volume" of the cell is $V=L_xL_y=40.2874r_2^2$. The mean interatomic spacing is $a=\sqrt{V/50}=0.8976r_2$.

Atoms of mass $m=10^{-22}$ g interact along the sides of the rhombi by a potential $V(r,r_2;r_2)$ represented by the leading terms of the expansion of a Lennard-Jones potential about the equilibrium spacing r_2:

$$V(r,r_2;r_2)=\varepsilon[(r_2/r)^{12}-2(r_2/r)^6]$$
$$\approx -\varepsilon+\tfrac{1}{2}\gamma\delta_2^2-\tfrac{1}{3}\mu\delta_2^3+\tfrac{1}{4}\nu\delta_2^4\ , \tag{2}$$

where $\delta_2=(r-r_2)/r_2$. For the constants ε and r_2, numerical values appropriate to solid rare gases were chosen: $r_2=3\times10^{-8}$ cm, $\varepsilon=1.75\times10^{-14}$ erg. With these values one finds

$$\gamma=126\times10^{-14}\text{ erg},$$
$$\mu=10.5\gamma\ , \tag{3}$$
$$\nu=61.83\gamma\ .$$

Interaction along the short rhombus diagonals is modeled by anharmonic springs with the same strengths as for the sides of the rhombus, but of different equilibrium lengths. The corresponding potentials are $V(r,r_i;r_2)$:

$$V(r,r_i;r_2)=-\varepsilon+\tfrac{1}{2}\gamma\delta_i^2-\tfrac{1}{3}\mu\delta_i^3+\tfrac{1}{4}\nu\delta_i^4\ , \tag{4}$$

where $\delta_i=(r-r_i)/r_2$, $i=1,2,3$.

In our simulations we used the potential $V(r,r_i;r_2)$ both in its complete form (4) (hereinafter referred to as anharmonic springs) and in a shortened form, with $\mu=\nu=0$ (harmonic springs). It should be noted that even with harmonic springs the system has anharmonicity in the following sense: When an atom is displaced by a distance u in a direction perpendicular to a bond of length r_i, the length of this bond becomes $r=(r_i^2+u^2)^{1/2}$. The force exerted on the displaced atom by its bond partner will be nonlinear in u because of the presence of the square root in r.

The aperiodic model (AM) is constructed from the periodic model. In each of the unit cells of the periodic model, we have chosen five atoms whose coordination number is six (see Fig. 3). Each of these atoms can be displaced to a new position of equilibrium, maintaining the orientational order of the bonds ("hexagonal flip"; see the description in Fig. 3). The aperiodic model is composed of eight different cells. The differences between the cells have been produced by moving, with probability $\frac{1}{2}$, five designated atoms in each cell to new equilibrium positions. Owing to this method of construction, the orientational order and topology are the same for the two models PM and AM, and in consequence, their densities of vibrational states are the same (see Sec. VII).

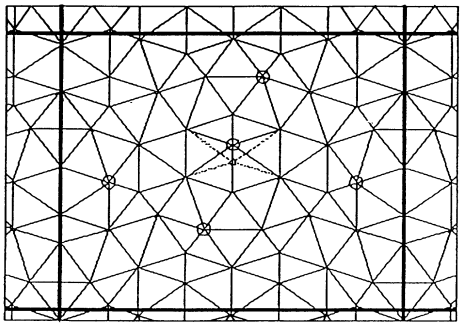

FIG. 3. Unit cell of the aperiodic model. The five atomic positions circled may be shifted to produce aperiodicity (see text). One of the shifted positions is shown by a small circle, and the shifted bonds are the dotted lines.

IV. METHOD OF SIMULATION

To obtain the thermal conductivity of the periodic and aperiodic models, we used the following procedure.

(1) All atoms were placed at their equilibrium positions and provided with initial velocities chosen randomly from a Maxwell distribution of temperature $2T$ (only kinetic, no potential energy). The atoms at the ends of the strip were fixed in their lattice positions. Periodic-boundary conditions were imposed in a direction perpendicular to the strip axis.

(2) The Beeman molecular-dynamics algorithm[14] was applied to solve the time-discretized equations of motion of the interacting atoms. The time step was about $\frac{1}{100}$ of the period of the highest-frequency harmonic mode of the system.

(3) As soon as the equipartition of energy between the kinetic and potential parts was established (after about 2000 times steps), the two ends of the sample were placed in contact with heat reservoirs of temperatures $T_1=1.5T$ and $T_2=0.5T$. In practice, this was achieved by transforming the 25 leftmost atoms into the high-temperature reservoir and the 25 rightmost atoms into the low-temperature reservoir. At each time step, the velocities of the atoms lying in the right and left reservoirs were scaled so that the desired temperature difference was maintained between the ends of the sample.[15]

(4) The process was continued until a uniform temperature gradient was obtained (180 000 time steps).

(5) The heat current $\mathcal{J}$ was calculated by two methods: (a) by determining the amount of energy entering (or leaving) the system per unit time,

$$\mathcal{J}_x=\frac{\Delta E}{A\,\Delta t}\ , \tag{5}$$

where A is the cross section of the system, and (b) by the formula[16]

$$\mathcal{J}=V^{-1}\left[\sum_{i=1}^{N}\mathbf{v}_iE_i+\tfrac{1}{4}\sum_{i=1}^{N}\sum_{j=1}^{N}(\mathbf{r}_i-\mathbf{r}_j)[\mathbf{F}_{ij}\cdot(\mathbf{v}_i+\mathbf{v}_j)]\right]\ , \tag{6}$$

where $\mathbf{r}_i$, $\mathbf{v}_i$, and E_i are, respectively, the position, veloci-

ty, and energy of atom i, $\mathbf{F}_{ij}$ is the force exerted by atom j on atom i, and V is the volume of the system (in our two-dimensional case, V is the area of the system). The mean value of $\mathcal{J}$ was calculated during 180 000 time steps. In the steady state, (5) and (6) give identical results for $\mathcal{J}_x$ within the accuracy of the calculation. The estimation of the accuracy is given by the transverse current $\mathcal{J}_y$ calculated from (6). Ideally the transverse current should be zero; in practice, it fluctuates during the simulation, but its value did not exceed 8% of $\mathcal{J}_x$.

(6) The thermal conductivity κ was calculated from

$$\mathcal{J}_x = -\kappa \frac{dT}{dx} , \tag{7}$$

where x is the longitudinal direction of the strip. The temperature gradient dT/dx was determined by a linear fit to the temperature profile far from the boundaries, the latter being deduced from the energy of layers of atoms perpendicular to the heat flux. Each layer contained 25 atoms (one-half of the unit cell).

V. THERMAL CONDUCTIVITY OF THE PERIODIC AND APERIODIC MODELS

The temperature profile for the aperiodic model with harmonic springs is shown in Fig. 4, curve *a*. The temperature is a linear function of position. The profiles for both models with anharmonic springs (not shown here) are also linear. The profile for the periodic model with harmonic springs is shown in Fig. 4, curve *b*. The temperature is only a linear function of position away from the boundaries. This fact is due to the boundary resistance of the thermal contact between the thermal reservoir and bulk. The boundary resistance does not depend on the size of the system. This is reflected in the fact that the length of the boundary regions, where the temperature profile is not linear, is independent of the length of the sample at a given temperature (see Fig. 4, curves *b* and *c*). A boundary resistance exists for the aperiodic model also, but since at 40 K the thermal resistance of the bulk is about twice as large as that for the periodic model, its effect is not visible in Fig. 4(a) (for further discussion of the boundary resistance and its influence on size dependence, see Appendix B). Using only the linear part of the temperature profile to calculate the thermal gradient dT/dx, we can use the formula (7) to find the thermal conductivity κ.

Figure 5 allows a comparison of the thermal conductivities as functions of temperature T of the periodic and aperiodic models. The thermal conductivity of the periodic model with harmonic springs is high and decreases when the temperature increases, as in a crystal. The introduction of harmonic terms in (4) reduces the conductivity by a factor of 2 at 10 K, but at high T the two curves converge.

The destruction of the periodicity, accomplished by displacing 5% of the atoms as explained in Sec. III (see Fig. 3), reduces the thermal conductivity by a factor of 3 at 10 K. The conductivity of the aperiodic model increases with temperature until saturation at about 60 K. This behavior of the thermal conductivity is observed experimentally in amorphous solids.

In order to verify the results presented in Fig. 5, we have studied the effects of varying the anharmonicity parameters μ and ν in the formula (4) for thermal conductivity at constant temperature. The thermal conductivities for different values of the anharmonic parameter are shown in Fig. 6. Since the higher the temperature, the larger the vibrational amplitudes of the atoms, and hence the higher the anharmonicity, Fig. 6 confirms the results presented in Fig. 5.

Although our simulation does not aim to describe any particular material, it is interesting to compare our results with experiment. Combining (5) and (7), we obtain, for the thermal conductivity $\kappa(2D)$ of the two-dimensional model,

$$\kappa(2D) = \frac{\Delta E}{A\,\Delta t\, dT/dx} , \tag{8}$$

where A is the cross section of the system, which is one dimensional in our case. To obtain the corresponding thermal conductivity $\kappa(3D)$ of a three-dimensional system, we divide the right-hand side of (8) by the lattice

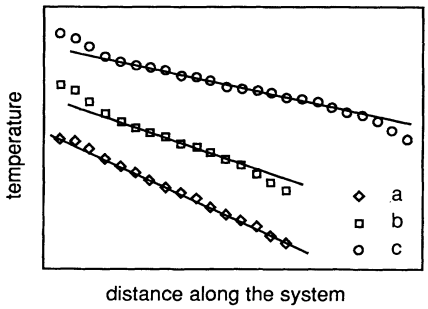

FIG. 4. Temperature profiles for systems with harmonic springs at $T=40$ K. For clarity the profiles are shifted in the vertical direction: (a) aperiodic model, 8 cells; (b) periodic model, 8 cells; and (c) periodic model, 12 cells. Note that the regions in which the profile is not linear have the same lengths in (b) and (c).

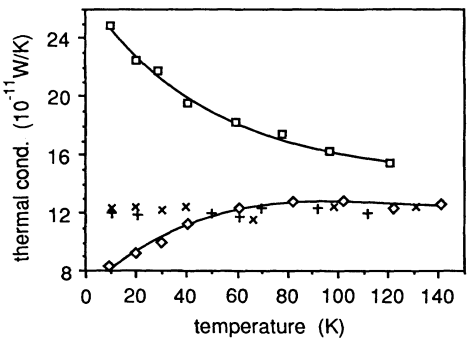

FIG. 5. Thermal conductivity as a function of temperature for systems consisting of eight unit cells each: periodic model with harmonic springs (□), aperiodic model with harmonic springs (◇), periodic model with anharmonic springs (×), and aperiodic model with anharmonic springs (+).

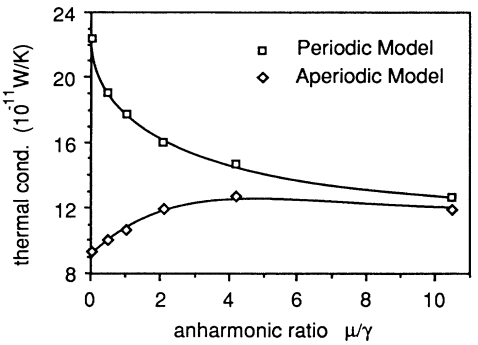

FIG. 6. Thermal conductivity at $T=20$ K as a function of the strength of the anharmonic terms in Eq. (4). The abscissa is the ratio μ/γ, and the ratio μ/v is held constant.

constant a ($a=0.8976r_2=2.7\times10^{-8}$ cm). This simulates a two-dimensional sample cross section. With $\kappa(2D)=12\times10^{-11}$ W/K from Fig. 5, we arrive at $\kappa(3D)=4.4$ mW/cmK, which is close to the values obtained for several amorphous solids (see Fig. 1).

VI. PROPAGATION OF SOUND

We have determined the sound velocity by simulating the introduction of a shock wave into the system. Initially, all the atoms were immobile at their equilibrium positions. At the instant $t=0$, five atoms at one end of the system were shifted from their equilibrium positions by a distance $d=10^{-10}$ cm ($=0.0033r_2$) toward the interior and then the system was left to evolve freely. We calculated the local energy at each site and observed how it changed with time. The result is shown in Fig. 7. One can see waves propagating at constant velocity $v=1250\pm100$ m/s (the same for both models, PM and AM).

In two dimensions the kinetic formula for the thermal conductivity is given by

$$K=\tfrac{1}{2}Cvl\ , \tag{9}$$

with the specific heat $C=2nk_B$ (n is the number of atoms per unit surface; in our case, $n=50/V=1.38\times10^{15}$ cm^{-2}), v the velocity of sound, and l the mean free path. With the sound velocity $v=1250$ m/s and the value $\kappa=12\times10^{-11}$ W/K from Fig. 5, one obtains the mean free path $l=5\times10^{-8}$ cm, which is about twice the mean interatomic distance a. We have thus reproduced the limiting thermal conductivity [see formula (1)].

VII. VIBRATIONAL PROPERTIES

To explain the differences in the behavior of the thermal conductivity of the periodic and aperiodic models, we calculated the eigenvectors and eigenvalues of the dynamical matrices (obtained from the equations of motion in the harmonic approximation) of both models. Periodic-boundary conditions were imposed in both directions. The density of states of the periodic model is shown in the histogram of Fig. 8. For the aperiodic model, the histogram is not significantly different from that for the periodic model. This is consistent with the observation that it is the local structure that determines the gross features of the density of states.[17] Both models have the same local structure and thus very similar densities of states. It follows that the difference in the thermal conductivities of the periodic and aperiodic models cannot be attributed to a difference in the densities of states. It is therefore likely that the density of states of an amorphous solid is not responsible for its thermal conductivity above the plateau.

Examination of the eigenvectors of the dynamical matrix (see Fig. 9) shows that the normal modes of the periodic model are extended and periodic (i.e., the distribution of the amplitude of vibration is periodic in space). In the aperiodic model, some of the high-frequency modes are strongly localized, and none of them is periodic (see Fig. 10). To obtain a quantitative measure of localization, we calculated the inverse participation ratio (R_{IP}) defined for each eigenvector $\mathbf{y}$ as[18]

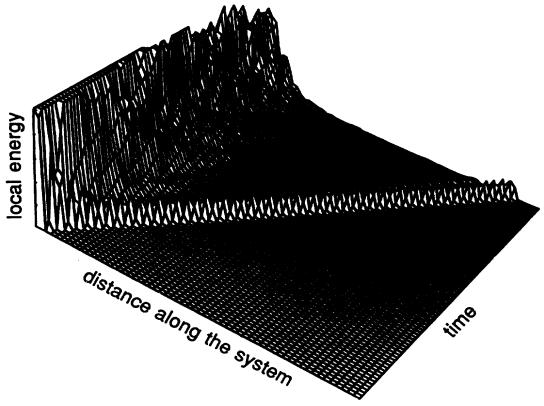

FIG. 7. Evolution of the local energy as a function of position along the periodic model composed of 30 unit cells (1500 atoms). Anharmonic springs. Waves propagating at a constant velocity are clearly seen.

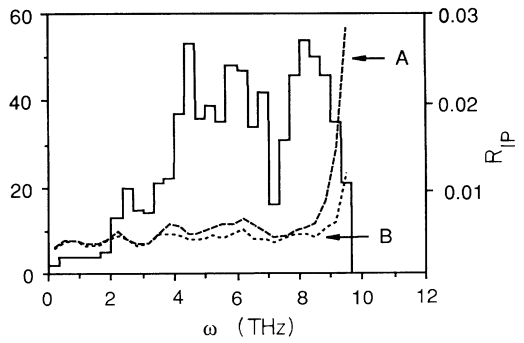

FIG. 8. Number of vibrational states per $\Delta\omega$ of the 400-atom periodic model as a function of the frequency ω (left scale). The mean inverse participation ratio R_{IP} of groups of eigenstates within $\Delta\omega$ are plotted for the aperiodic (A) and periodic (B) models (right scale). $\Delta\omega=0.333$ THz.

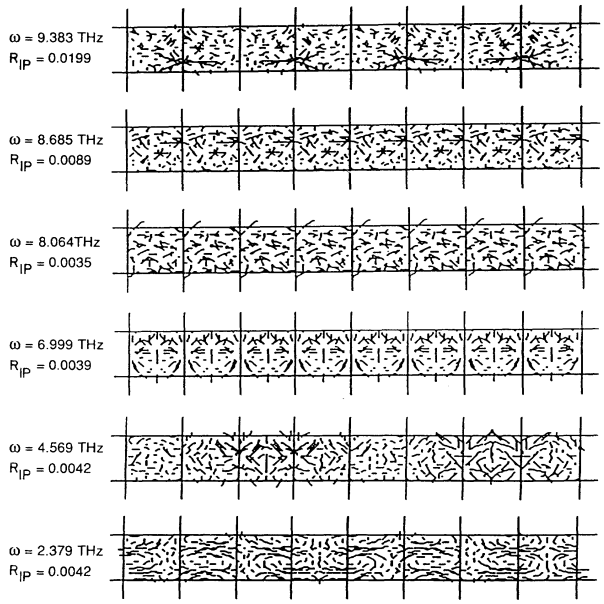

FIG. 9. Typical examples of the harmonic modes of the periodic model. The bars are the amplitudes of vibration of each atom moving in the mode.

$$R_{\mathrm{IP}}(\mathbf{y})=\frac{\sum_i y_i^4}{(\sum_i y_i^2)^2} \ . \tag{10}$$

The definition (10) implies that for vibrations localized on one site, $R_{\mathrm{IP}}=1$, whereas for uniformly spread vibrations $R_{\mathrm{IP}}=1/N$, where N is the number of atoms. Figure 8 shows that the R_{IP} increases with frequency and is larger for the aperiodic model. It should be noted that, even if

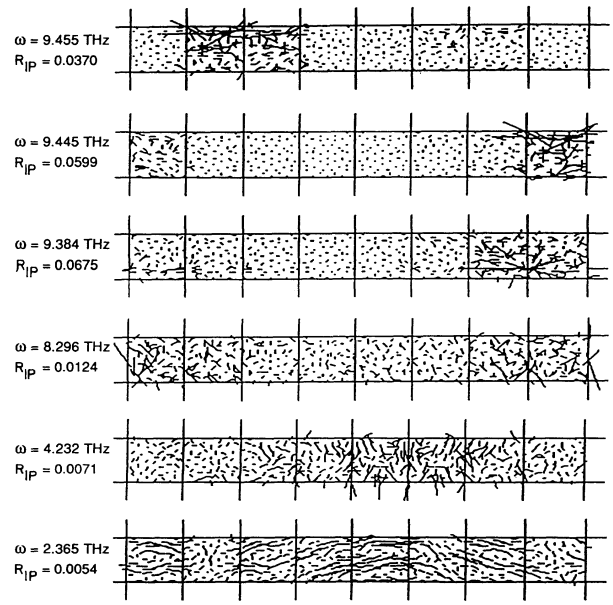

FIG. 10. Typical examples of the harmonic modes of the aperiodic model.

the R_{IP}'s for high-frequency modes of the periodic model are bigger than those for smaller frequencies, this does not mean that these modes are localized. They are extended, as can be seen in Fig. 9, where the periodicity of the modes is also clearly visible. On the other hand, the higher R_{IP}'s for normal modes of the aperiodic model imply localization (see Fig. 10).

One sees that the aperiodicity of the aperiodic model involves the localization of vibrations. Now we are able to explain the difference in the thermal conductivities of the periodic and aperiodic models.

Owing to lack of periodicity, some of the modes become localized. A localized mode does not contribute appreciably to the heat current, because to do so a mode must have a sizable amplitude at both ends of the sample. Consequently, energy does not propagate well in the aperiodic model. A localized mode can transfer its energy to another mode localized elsewhere, or to an extended mode, by means of anharmonic interactions, contributing to the heat current in this way. Even the extended modes of the aperiodic model cannot transfer heat as effectively as those of the periodic model. Indeed, in solids, energy propagates in the form of wave packets, which are superpositions of the stationary normal modes. In a periodic structure, a given wave packet can propagate freely because it is composed of the same normal modes everywhere. In the aperiodic model, a wave packet has to change its composition while moving, because the normal modes are not periodic, and this change is possible only through anharmonicity. Thus anharmonicity facilities heat transfer in the aperiodic model (see Fig. 11).

On the other hand, modes localized near the ends of the sample prevent a rapid drop in temperature close to the boundaries, thereby increasing the thermal gradient. The anharmonicity which increases the heat current diminishes the thermal gradient in the aperiodic model (see Fig. 12). It follows that the thermal conductivity, being the heat current divided by the temperature gradient, increases with anharmonicity (see Fig. 6).

In the periodic model, where all modes are extended and periodic, anharmonicity introduces scattering, which diminishes the thermal conductivity, as in crystals. Thus the difference in the behavior of the thermal conductivi-

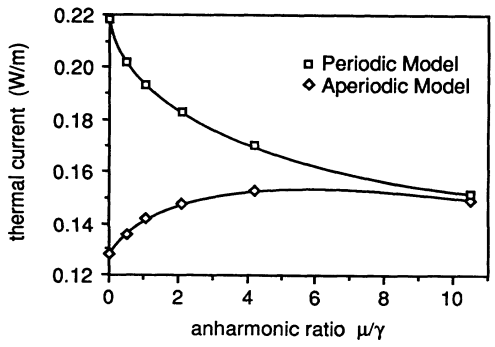

FIG. 11. Thermal current at $T=20$ K as a function of anharmonicity. The abscissa is the ratio μ/γ in Eq. (4), and the ratio μ/ν is held constant.

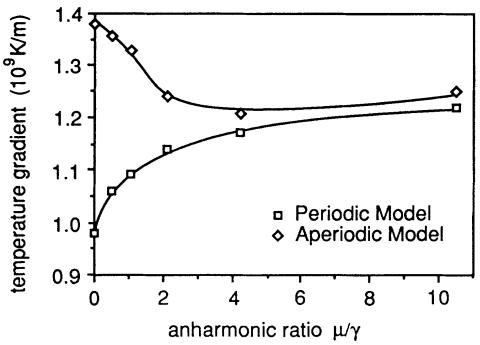

FIG. 12. Thermal gradient at $T=20$ K as a function of anharmonicity.

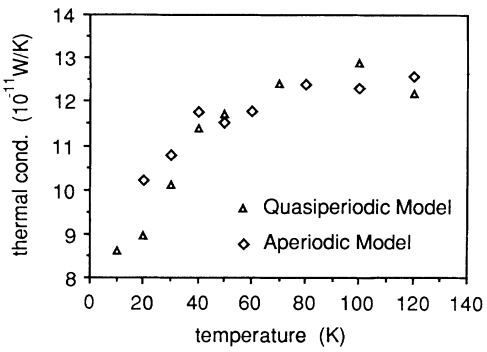

FIG. 13. Thermal conductivities of the quasiperiodic and aperiodic models (550 atoms).

ties of the periodic and aperiodic models is due to the difference in localization and periodicity of the normal modes.

VIII. THERMAL CONDUCTIVITY OF THE QUASIPERIODIC MODEL

In the preceding sections, we showed that lack of periodicity and the localization of vibrations which this entails can explain the thermal conductivity of amorphous solids. To verify this conclusion further, we undertook the simulation of a model which is very similar to the periodic and aperiodic models, but is quasiperiodic in one direction. The questions were the following.

(1) What influence does the quasiperiodicity have on the thermal conductivity?

(2) Is this influence different from that of a simple aperiodicity?

We constructed the quasiperiodic model (QM) as an approximant of the Penrose tiling with $F_x=\tau$ and $F_y=\frac{2}{1}$, τ being the golden number (see Appendix A). For the grid parameters, we chose $\gamma_i=0.2$, $i=1,\ldots,5$ [see Appendix A, Eq. (A1)]. We added bonds along the short diagonals of the rhombi, as in the periodic and aperiodic models (see Sec. III). The infinite quasiperiodic strip was cut in such a way that the quasiperiodic model contained 550 atoms. Here we chose the size of the system to be larger than that of the PM and AM studied earlier because this facilitates the detection of quasiperiodicity, which remains invisible if the system is too small. In order to make a direct comparison of the conductibilities of the aperiodic and quasiperiodic models, we repeated our simulation for the AM with 11 unit cells (550 atoms). The linear dimensions of these two models (AM and QM) with 550 atoms are identical.

Since the length of the models with 550 atoms is larger than that of the models with 400 atoms, more time steps were necessary in order to obtain a stable temperature profile. We waited 500 000 time steps before recording data for a further 500 000 time steps (for models with 400 atoms, we used 180 000 time steps; cf. Sec. IV). Figure 13 shows that the thermal conductivities of the aperiodic and quasiperiodic models are the same. Thus the effect of the quasiperiodicity on the thermal conductivity is the same as that of a simple aperiodicity. Nevertheless, it is possible that the small size of the model (550 atoms) did not allow the quasiperiodicity to show any effect in the results.

IX. LOCALIZED VIBRATIONAL MODES, ANHARMONICITY, AND THE SPECTRAL INTENSITY

In Fig. 5 one sees that the two curves of the thermal conductivities of the PM and AM with harmonic springs converge to the common value 12×10^{-11} W/K, but the thermal conductivity of the AM saturates at about 60 K, while that of the PM has still not reached its high-temperature limit value even at 120 K. The reason for this difference is that the anharmonicity is stronger in the aperiodic model than in the periodic model, even if the two models are very similar (as described in Sec. III) and the interatomic interactions (the springs) are exactly the same. To understand this, let us look at Figs. 9 and 10. It is clearly visible that the high-frequency modes of the AM are strongly localized, while those of the PM are extended. In a classical system, all modes have the same energy (equipartition of energy), and so, in particular, a localized mode has the same energy as an extended one. Now, in a localized mode, only some of the atoms move, and their displacements must be much larger than those of atoms moving in an extended mode, if the two modes are to have the same energy, and larger displacements mean larger anharmonicity. These arguments are also valid for a quantum system (where not all of the modes are excited at low temperatures), but they should only be applied to modes of (almost) the same frequency. Thus we see that the anharmonicity is stronger in the aperiodic model than in the periodic model because the vibrational localization involves anharmonicity.

To verify this statement, we performed a molecular-dynamics simulation.

(1) In a system (PM or AM) with harmonic springs (we recall that harmonic springs do not imply harmonic approximation; see Sec. III), we excited only one harmonic mode found from the diagonalization of the dynamical matrix of the system in the harmonic approximation.

This was done by choosing the initial displacements of the atoms equal to the corresponding components of a given eigenvector of the dynamical matrix and putting the initial velocities equal to zero.

(2) We allowed the system to evolve freely during ten periods of vibration of the harmonic mode, and we looked at the energy of the mode. The energy of the kth mode is given by

$$E_k = \frac{P_k^2}{2m} + \frac{m}{2}\omega_k^2 Q_k^2 , \tag{11}$$

where

$$Q_k = \sum_{i=1}^{N} (u_i^x q_k^{i,x} + u_i^y q_k^{i,y}) , \tag{12}$$

$$P_k = m \sum_{i=1}^{N} (v_i^x q_k^{i,x} + v_i^y q_k^{i,y}) . \tag{13}$$

In (12) and (13), $\mathbf{q}_k = (q_k^{1,x}, \ldots, q_k^{N,x}, q_k^{1,y}, \ldots, q_k^{N,y})$ is the kth eigenvector of the dynamical matrix, u_i^α (v_i^α) is the αth component of the displacement (velocity) of the ith atom, and m is the atomic mass. Figure 14 presents the results of this simulation. One notes that the higher the R_{IP} of a mode, the faster the mode loses its energy. This result confirms the statement that higher vibrational localization involves higher anharmonicity. However, the situation in which only one harmonic mode is excited is rather artificial, and this simulation does not describe completely what happens when *all* the modes are present.

To study the effects of anharmonicity further, we examined the spectral intensities which are the Fourier transforms of the time evolution of the vibrational modes.[19] The time evolution of the kth vibrational mode is given by (12).

To obtain correct results for the spectral intensities from the time evolution of a classical system at constant temperature, the energy should be uniformly distributed over all modes. At high temperatures ($T \gtrsim 100$ K), the equipartition of energy can be rapidly obtained by placing the atoms at their equilibrium positions and providing them with initial velocities chosen randomly from the Maxwell distribution. Owing to the anharmonic coupling, after a certain time (we used 2000 time steps), the energy was redistributed among the modes. This procedure fails at low temperatures, because of the small value of the anharmonic coupling. For this reason we adopted the following procedure.

(1) All atoms were placed at their equilibrium positions and provided with initial random velocities chosen from a Maxwell distribution of temperature $2T$. We chose $T = 400$ K.

(2) The system was allowed to evolve freely during 2000 time steps.

(3) We cooled the system to a required temperature by multiplying the velocities by a factor of 0.992 at every tenth time step (for example, to attain the temperature 10 K, 4600 time steps were necessary).

(4) As soon as the required temperature was attained, we allowed another 5000 time steps of free evolution before starting to record data.

That this procedure proved to be effective was shown by the independence of the results on details of preparation such as different initial random velocities or the scaling factor equal to 0.995 instead of 0.992.

After having obtained the equipartition of energy at a required temperature, a run of 399 360 time steps was made. The deviations of each atom from its equilibrium position were recorded every 26 time steps, in order to find the time evolution of the modes according to (12).

The spectral intensities[20] of some modes of the periodic and aperiodic models are shown in Figs. 15–17. The spectral intensities of the modes of the periodic model are all well-defined single peaks, the position and linewidth of

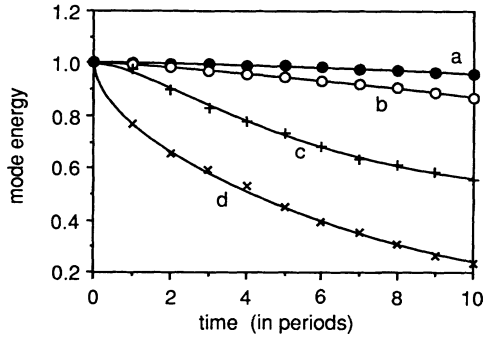

FIG. 14. Decay of harmonic modes after the initial excitation. Initially, only one mode was excited. One notes that the higher the R_{IP} of a given mode, the faster the mode decays. (a) periodic model, mode 20, $\omega = 9.335$ THz, $R_{IP} = 0.005$; (b) periodic model, mode 10, $\omega = 9.390$ THz, $R_{IP} = 0.022$; (c) aperiodic model, mode 7, $\omega = 9.444$ THz, $R_{IP} = 0.041$; (d) aperiodic model, mode 15, $\omega = 9.383$ THz, $R_{IP} = 0.087$ (modes of each model are numbered in order of decreasing frequency).

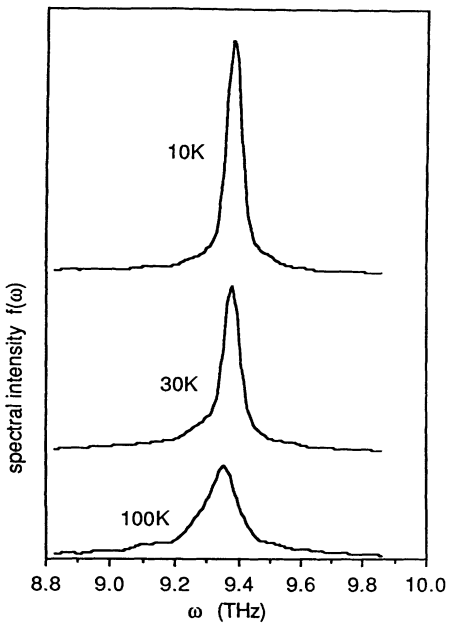

FIG. 15. Spectral intensity of the tenth mode of the periodic model, $\omega = 9.390$ THz, $R_{IP} = 0.022$.

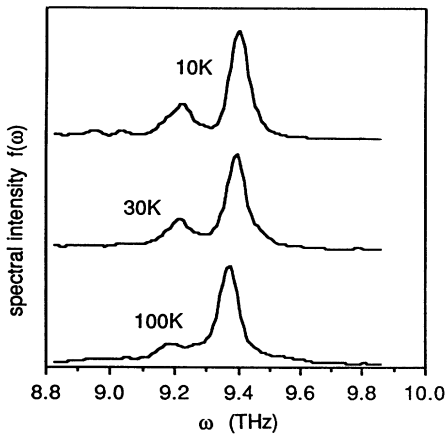

FIG. 16. Spectral intensity of the seventh mode of the aperiodic model, $\omega=9.444$ THz, $R_{IP}=0.041$.

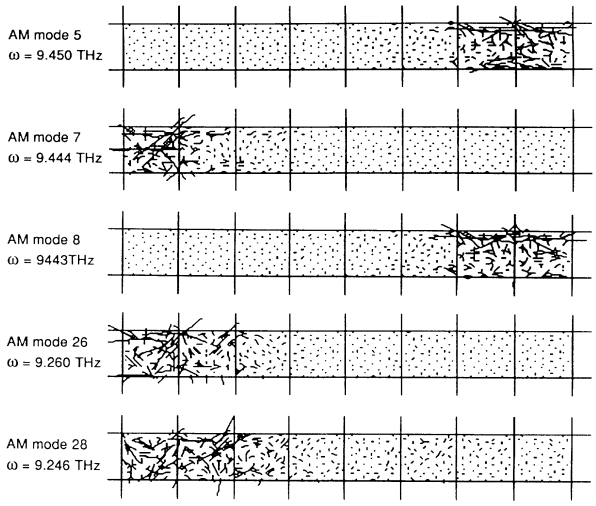

FIG. 18. Harmonic modes of the aperiodic model with fixed ends.

which are in qualitative agreement with experimental observations,[21,23] numerical simulations,[24,25] and theoretical predictions for crystals:[26,27] the linewidth increases with temperature, and the position of maximum shifts to lower frequencies. The spectral intensities of the localized modes of the aperiodic models are quite different. Some of them have additional peak (see Fig. 16). Other are similar to those of the modes of the periodic model, but there are some humps visible on the graphs (Fig. 17) which do not occur in the PM. We can see that localized harmonic modes are not always well-defined excitations of the aperiodic model with harmonic springs, even at low temperature. To explain this we did another molecular-dynamics simulation. We excited a localized harmonic mode in the aperiodic model with harmonic springs, and we examined the energy of this mode together with the energies of the other modes. In this way we were able to see with which modes a given mode interacts most strongly.

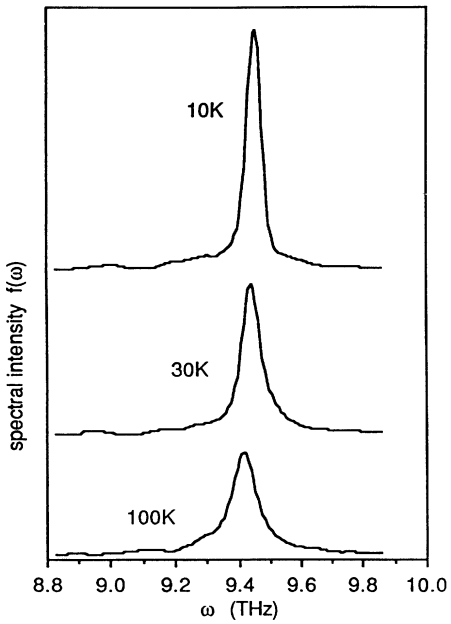

FIG. 17. Spectral intensity of the fifth mode of the aperiodic model, $\omega=9.445$ THz, $R_{IP}=0.035$. Small humps are visible at frequencies near 9 and 9.3 THz.

We observed that some modes took much more energy from the initially excited one than others did. This implies that they interact much more strongly with the excited mode than do the others. For example, when we excited mode 7 of the aperiodic model (its spectral intensity is shown in Fig. 16), after ten periods of its vibrations, 12% of its initial energy went to modes 26 and 28, no energy went to modes 5 and 8, and very little to each of the others, 55% remaining in mode 7. The frequencies of modes 26 and 28 correspond to the position of the additional peak at $\omega\approx 9.2$ THz in Fig. 16. Thus the existence of the additional peaks is explained. But why does mode 7 interact strongly with modes 26 and 28, while its interaction with modes 5 and 8 is very weak? Figure 18 gives an immediate answer: Modes that are localized at the same place interact strongly, even if their frequencies are not very close; modes that are localized at different places interact very weakly, even if their frequencies are very close.

Thus we arrive at the following conclusions.

(1) Vibrational localization involves strong anharmonicity.

(2) The strength of the anharmonic interaction between localized modes is determined predominantly by the position of localization and not by the distance between their frequencies. This fact is reflected in the spectral intensities of the localized modes, which have several peaks instead of only one.

X. DISCUSSION

Our results for the thermal conductivity are in agreement with the predictions of Jagannathan, Orbach, and Entin-Wohlman[6] (cf. Sec. II)—the conductivity first in-

creases linearly with temperature and then saturates when the lifetime of the localized modes becomes of the order of the period of their vibrations. Indeed, the mean lifetime is given by $\vartheta \approx l/v = (5\times10^{-10}\ \text{m})/(1250\ \text{m/s}) \approx 4\times10^{-13}\ \text{s}$ (l is the mean free path, and v is the velocity of sound), the period of the localized vibrations is

$$\Theta = \frac{2\pi}{\omega} = \frac{2\pi}{9.5\times10^{12}\ \text{s}^{-1}} \approx 6.6\times10^{-13}\ \text{s} ,$$

and one finds $\vartheta \approx 0.6\Theta$. The results of our simulation agree particularly with the note of Jagannathan, Orbach, and Entin-Wohlman,[6] that even if their calculations were based on the model of fractons, the results should also be valid for more conventional localized vibrations. Indeed, the connectivities in the periodic and aperiodic models are the same, so that, even if one imagines that the AM is "fractal," the PM should also be "fractal." This supports the idea that, as long as vibrations are localized, the exact form of their wave functions is not important for the thermal conductivity.

Our results show that the model of Karpov and Parshin,[7] whereby the increase of the thermal conductivity is attributed to the decrease of the population of two-level systems (see Sec. II), is not indispensable to explain the thermal conductivity of glasses above the plateau. Indeed, in the aperiodic model, there are no two-level systems (there are no double-well potentials, and moreover the system is classical), but nevertheless the conductivity increases with temperature. Thus we conclude that the mechanism proposed by Karpov and Parshin can, at most, be added to that predicted by Jagannathan, Orbach, and Entin-Wohlman.

The mechanism proposed by Kittel[8] (in which the thermal conductivity increases with the specific heat; see Sec. II) and confirmed numerically by Allen and Feldman[9] should also be considered as additional to that of Jagannathan, Orbach, and Entin-Wohlman. Indeed, our molecular-dynamics simulation is classical and the specific heat of the aperiodic model is constant—thus the increase of the thermal conductivity cannot be attributed to the increase of the specific heat. It is not surprising, then, that Allen and Feldman found the thermal conductivity of their model of amorphous silicon smaller than that measured experimentally—their calculations, done in harmonic approximation, neglected (apart from the contribution of long-wavelength vibrations) the increase of the conductivity due to anharmonicity.

The thermal conductivity of the quasiperiodic model studied in Sec. VIII is the same as that of the aperiodic model. This suggests that the quasiperiodicity affects the thermal conductivity in the same way as a simple aperiodicity. Nevertheless, the small size of the model does not allow a definitive conclusion to be drawn about the thermal conductivity of quasicrystals.

The results of Sec. IX show that vibrational localization in amorphous solids involves strong anharmonicity which cannot be treated by perturbation calculation, even at low temperatures. Thus any realistic description of thermal properties of amorphous solids must include a full treatment of anharmonicity and not consider it as a small correction to the harmonic forces. We believe that this strong anharmonicity, which is due to the vibrational localization, may be responsible for the low-temperature thermal properties of glasses.[28,29]

ACKNOWLEDGMENTS

The author wishes to thank Professor P. Erdös for helpful comments and Dr. F. Gähler for providing the computer program which generates approximants of the Penrose pattern. The support of the Swiss National Science Foundation through Grant No. 20.28846.90 is gratefully acknowledged.

APPENDIX A: CONSTRUCTION OF APPROXIMANTS OF THE PENROSE TILINGS BY THE MULTIGRID METHOD

Let $\{\mathbf{g}_i\}_{i=1,\ldots,5}$ be a star of unit vectors pointing to the vertices of a regular pentagon. These are called grid vectors. The grid G_5 is defined as an ensemble of five arrays of equidistant parallel lines orthogonal to the vectors $\mathbf{g}_i$:

$$G_5 = \{\mathbf{x}\in E^2 | \mathbf{x}\cdot\mathbf{g}_i - \gamma_i = k_i;\ i=1,\ldots,5,\ k_i\in\mathbb{Z}\} . \quad \text{(A1)}$$

The grid parameters $\gamma_i\in\mathbb{R}$ define translations of the arrays relative to the origin.

Let us assign a vector $\mathbf{K}(\mathbf{y})\in\mathbb{Z}^5$ to every point $\mathbf{y}\in E^2$, defined by the components $K_i(\mathbf{y})$ given by

$$K_i(\mathbf{y}) = \lceil \mathbf{y}\cdot\mathbf{g}_i - \gamma_i \rceil, \quad i=1,\ldots,5, \quad \text{(A2)}$$

where $\lceil x \rceil = \min\{n\in\mathbb{Z} | n\geq x\}$. Let $\mathbf{x}_0$ be an intersection point of two grid lines and $U(\mathbf{x}_0)$ a small neighborhood of $\mathbf{x}_0$ containing no other intersection points. From (A1) and (A2) it follows that on $U(\mathbf{x}_0)$ the vector $\mathbf{K}(\mathbf{y})$ takes on four different values $\mathbf{K}(\mathbf{x}_0, j)$, $j=1,\ldots,4$. The four vectors

$$\mathbf{P}(\mathbf{x}_0, j) = \sum_{i=1}^{5} K_i(\mathbf{x}_0, j)\mathbf{g}_i, \quad j=1,\ldots,4 , \quad \text{(A3)}$$

point to the vertices of one of the two Penrose rhombi.[30] The set of rhombi defined by all intersection points form a perfect tiling.

This method can be generalized.[30] The vectors $\mathbf{g}_i$ in the formula (A3) are not necessarily the same as those in (A1). One can associate an arbitrary vector $\mathbf{t}_i$ with each vector $\mathbf{g}_i$. The only restriction is that for every couple of indices (i_1, i_2) the corresponding pairs of vectors $(\mathbf{g}_{i_1}, \mathbf{g}_{i_2})$ and (t_{i_1}, t_{i_2}) span a surface of the same orientation. Instead of (A3) one can write

$$\mathbf{P}(\mathbf{x}_0, j) = \sum_{i=1}^{5} K_i(\mathbf{x}_0, j)\mathbf{t}_i, \quad j=1,\ldots,4 . \quad \text{(A4)}$$

To obtain the Penrose tiling, the vectors $\mathbf{t}_i$, $i=1,\ldots,5$, are given (with accuracy to the normalization factors) by

$$\mathbf{t}_1=\begin{bmatrix}0\\2\end{bmatrix},\quad \mathbf{t}_2=\begin{bmatrix}2\tau-1\\\tau-1\end{bmatrix},\quad \mathbf{t}_3=\begin{bmatrix}3-\tau\\-\tau\end{bmatrix},$$
$$\mathbf{t}_4=\begin{bmatrix}\tau-3\\-\tau\end{bmatrix},\quad \mathbf{t}_5=\begin{bmatrix}1-2\tau\\\tau-1\end{bmatrix}, \tag{A5}$$

where $\tau=(1+\sqrt{5})/2\simeq 1.618\,03$ is the golden number.

If one chooses the vectors $\mathbf{g}_i$ in (A1) identical to the vectors $\mathbf{t}_i$ given by (A5), using (A1), (A2), and (A4), one obtains the ideal Penrose tiling (quasiperiodic, self-similar).

To obtain periodic approximants of the Penrose tiling, one utilizes rational approximants of the golden number. The golden number is the limit of the series

$$\tau=\lim_{i\to\infty}\frac{f_{i+1}}{f_i}, \tag{A6}$$

where f_i is the ith Fibonacci number. The two first Fibonacci numbers are 1, $f_1=f_2=1$, the ith number, $i>2$, is defined as $f_i=f_{i-2}+f_{i-1}$. Consecutive approximants of the golden number are thus $\frac{1}{1}=1$, $\frac{2}{1}=2$, $\frac{3}{2}=1.5$, $\frac{5}{3}=1.667$, $\frac{8}{5}=1.6$, $\frac{13}{8}=1.625$, etc. Let us define $F_i=f_{i+1}/f_i$. In order to obtain periodic approximants of the Penrose tiling, one defines the vectors $\mathbf{g}_i$ as follows [cf. (A5)]:

$$\mathbf{g}_1=\begin{bmatrix}0\\2\end{bmatrix},\quad \mathbf{g}_2=\begin{bmatrix}2F_x-1\\F_y-1\end{bmatrix},\quad \mathbf{g}_3=\begin{bmatrix}3-F_x\\-F_y\end{bmatrix},$$
$$\mathbf{g}_4=\begin{bmatrix}F_x-3\\-F_y\end{bmatrix},\quad \mathbf{g}_5=\begin{bmatrix}1-2F_x\\F_y-1\end{bmatrix}, \tag{A7}$$

where $x,y=3,4,5,6,\ldots$. Let us note that, in general, different components of the vectors $\mathbf{g}_i$ can utilize different approximants of the golden number; i.e., x and y in (A7) may not be the same. In this way one obtains periodic approximants of the Penrose tiling with different periods in each direction. In particular, we used $F_x=F_y=\frac{2}{1}$ to construct the unit cell of the periodic model (Sec. III) and $F_x=\tau$ and $F_y=\frac{2}{1}$ for the strip, quasiperiodic in the x direction (Sec. IX).

APPENDIX B: BOUNDARY RESISTANCE AND SIZE DEPENDENCE

To study how the size of the system can influence the results for thermal conductivity, we performed simulations for the periodic and aperiodic models of different lengths (i.e., composed of different numbers of the "unit cells"). We found that, at a given temperature, the length dependence of the thermal conductivity κ [defined by Eq. (7)] is well described by

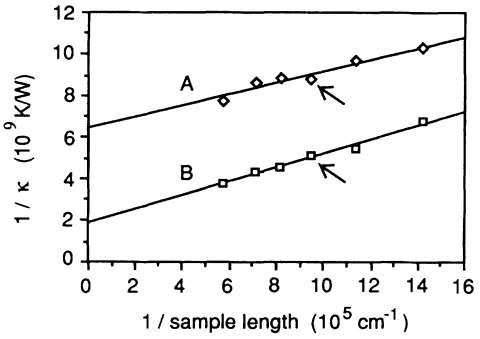

FIG. 19. Length dependence of the thermal conductivity of the aperiodic (line A) and periodic (line B) models with harmonic springs at 40 K. Data points indicated by the arrows are those used in Fig. 5.

$$\frac{1}{\kappa}=r+R_b/L, \tag{B1}$$

where r is the bulk thermal resistance per unit length and R_b is the boundary resistance. r and R_b are both independent of the length L. Owing to the presence of boundary resistance, the thermal conductivity κ increases with the length of the system and saturates at $\kappa(L=\infty)=1/r$. The plot of $1/\kappa$ versus $1/L$ for the periodic model with harmonic springs is shown in Fig. 19, line B. The slope is the boundary resistance, and the intersection of the line with the vertical axis gives the inverse of the thermal conductivity of the bulk.

We found that the boundary resistance varied little with temperature; for instance, at 40 K it is about 10% smaller than at 20 K. One can expect the boundary resistance to be the same for both the periodic and aperiodic models. Indeed, the slopes of the two lines in Fig. 19 are very similar. It is clear then that increasing the length of the systems will not change the qualitative difference between the thermal conductivities of the periodic and aperiodic models. For this reason our simulations were limited to systems of fixed lengths, and in order to minimize the influence of size dependence on the conclusions, the properties of models of the same size were compared.

One could imagine that the vibrational localization (see Sec. VIII) might influence the size dependence of the thermal conductivity of the aperiodic model. Indeed, in a finite system, some of the localized modes may still have nonzero amplitudes at both ends of the system and so contribute directly to the heat conduction. The longer the system, the smaller the fraction of such modes. Thus one of the effects of the vibrational localization could be to diminish the thermal conductivity of the aperiodic model when the length of the system is increased. We did not observe such an effect in our simulations.

*Present address: Institute of Zoology and Animal Ecology, University of Lausanne, CH-1015 Lausanne, Switzerland.
[1]D. G. Cahill and R. O. Pohl, Phys. Rev. B **35**, 4067 (1987).
[2]R. C. Zeller and R. O. Pohl, Phys. Rev. B **4**, 2049 (1971).
[3]J. Michalski and P. Erdös, Solid State Commun. **72**, 967 (1989).
[4]S. Alexander, O. Entin-Wohlman, and R. Orbach, Phys. Rev. B **34**, 2726 (1986).
[5]S. Alexander and R. Orbach, J. Phys. (Paris) Lett. **43**, L-625 (1982).
[6]A. Jagannathan, R. Orbach, and O. Entin-Wohlman, Phys. Rev. B **39**, 13 465 (1989).
[7]V. G. Karpov and D. A. Parshin, Zh. Eksp. Teor. Fiz. **88**, 2212 (1985) [Sov. Phys. JETP **61**, 1308 (1985)].
[8]C. Kittel, Phys. Rev. **75**, 972 (1949).
[9]P. B. Allen and J. L. Feldman, Phys. Rev. Lett. **62**, 645 (1989).
[10]F. Wooten, K. Winer, and D. Weaire, Phys. Rev. Lett. **54**, 1392 (1985).
[11]D. G. Cahill, H. E. Fisher, T. Klitsner, E. T. Swartz, and R. O. Pohl, J. Vac. Sci. Technol. A **7**, 1259 (1989).
[12]R. Penrose, Bull. Inst. Math. Appl. **10**, 266 (1974).
[13]B. Grünbaum and G. C. Shephard, *Tiling and Patterns* (Freeman, New York, 1987).
[14]D. Beeman, J. Comput. Phys. **20**, 130 (1976).
[15]R. D. Mountain and R. A. MacDonald, Phys. Rev. B **28**, 3022 (1983).
[16]J. Ranninger, Phys. Rev. **140**, A2031 (1965).
[17]S. R. Elliott, *Physics of Amorphous Materials* (Longman, London, 1984).
[18]J. Canisius and J. L. van Hemmen, J. Phys. C **18**, 4873 (1985).
[19]In the literature (see, for example, Refs. 24 and 25), the spectral intensity is usually calculated from the Fourier transform of the velocity correlation function even when the dynamics of the system is determined by interatomic potentials, which are not necessarily harmonic. This is meaningful as long as harmonic modes are still reasonably well-defined excitations of the system, i.e., when the spectral intensity gives a well-defined peak. This is not the case for the localized modes of the aperiodic model (see Fig. 16), and so we preferred to calculate the spectral intensity directly from the Fourier transform of the displacements, which needs much more computer time, but does not use unjustified approximations.
[20]The spectral intensities obtained from the discrete Fourier transform are very spiky because of the finite size of the system, and it is necessary to smooth the plot by replacing each δ-like peak of height H by a Gaussian $He^{-(\omega/\sigma)^2}$. The width of the smooth peak thus obtained depends on the value of σ chosen, so that lifetimes found from the widths of the peaks can only be crude estimates. However, one can always *compare* the spectral intensities for different systems (as we did by comparing Figs. 15–17) or compare the calculated results with experiment, if σ is chosen to be equal to the resolution of the experiment (as was done in Refs. 24 and 25). We chose $\sigma=0.02$ THz.
[21]T. R. Hart, R. L. Aggarwal, and B. Lax, Phys. Rev. B **1**, 638 (1970).
[22]M. Balkanski, R. F. Wallis, and E. Haro, Phys. Rev. B **28**, 1928 (1983).
[23]J. Menéndez and M. Cardona, Phys. Rev. **29**, 2051 (1984).
[24]C. Z. Wang, C. T. Chan, and K. M. Ho, Phys. Rev. B **40**, 3390 (1989).
[25]C. Z. Wang, C. T. Chan, and K. M. Ho, Phys. Rev. B **42**, 11 276 (1990).
[26]R. F. Wallis, J. P. Ipatova, and A. A. Maradudin, Fiz. Tverd. Tela (Leningrad) **8**, 1064 (1966) [Sov. Phys. Solid State **8**, 850 (1966)].
[27]S. Narasimhan and D. Vanderbilt, Phys. Rev. **43**, 4541 (1991).
[28]J. Michalski, and P. Erdös, Phys. Rev. B **41**, 9534 (1990).
[29]J. Michalski and P. Erdös (unpublished).
[30]F. Gähler and J. Rhyner, J. Phys. A **19**, 267 (1986).

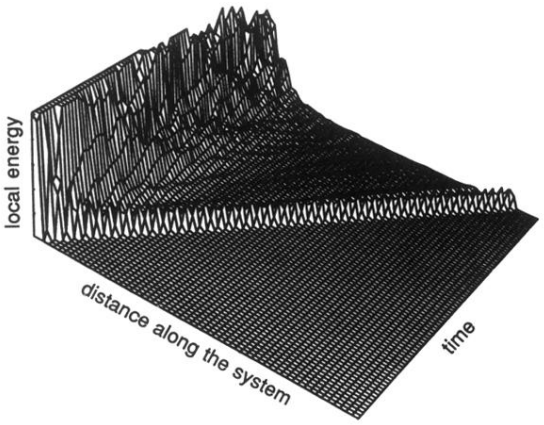

FIG. 7. Evolution of the local energy as a function of position along the periodic model composed of 30 unit cells (1500 atoms). Anharmonic springs. Waves propagating at a constant velocity are clearly seen.